INTERNATIONAL JOURNAL FOR NUMERICAL METHODS IN BIOMEDICAL ENGINEERING
Int. J. Numer. Meth. Biomed. Engng. 2010; **00**:1–21
Published online in Wiley InterScience (www.interscience.wiley.com). DOI: 10.1002/cnm

The role of the microvascular network structure on diffusion and consumption of anti-cancer drugs

P. Mascheroni[1], R. Penta [2*]

[1]*DICEA, Università di Padova, Via Marzolo 9, 35131 Padova, Italy*
[2]*Departamento de Mecanica de los Medios Continuos y T. Estructuras, E.T.S. de caminos, canales y puertos, Universidad Politecnica de Madrid, Calle Profesor Aranguren S/N, 28040, Madrid, Spain.*

SUMMARY

We investigate the impact of the tumor microvascular geometry on transport of drugs in solid tumors, in particular focusing on the diffusion and consumption phenomena. We embrace recent advances in the asymptotic homogenization literature starting from a double Darcy, double advection-diffusion-reaction system of partial differential equations which is obtained exploiting the sharp length separation between the intercapillary distance and the average tumor size. The geometric information on the microvascular network is encoded into effective hydraulic conductivities and diffusivities, which are numerically computed by solving periodic cell problems on appropriate microscale representative cells. The coefficients are then injected into the macroscale equations, which are solved for an isolated, vascularized spherical tumor. We consider the effect of vascular tortuosity on the transport of anti-cancer molecules, focusing on the Vinblastine and Doxorubicin dynamics, which can be considered a tracer and a highly interacting molecule, respectively. The computational model is able to quantify the performance of the treatment through the analysis of the interstitial drug concentration and the quantity of drug metabolized in the tumor. Our results show that both drug advection and diffusion are dramatically impaired by increasing geometrical complexity of the microvasculature, leading to non-optimal absorption and delivery of therapeutic agents. However, this effect apparently has a minor role whenever the dynamics are mostly driven by metabolic reactions in the tumor interstitium, i.e. for highly interacting molecules. In the latter case, anti-cancer therapies that aim at regularizing the microvasculature might not play a major role and different strategies are to be developed.

Received . . .

KEY WORDS: Asymptotic homogenization; Tumor microvasculature; Drug delivery; Advection-Diffusion-Reaction; Computational modeling.

1. INTRODUCTION

A tumor mass needs nutrients supply to grow beyond a certain size. This is achieved via the angiogenesis process, i.e. the tumor cells secrete factors that stimulate the formation of a new vasculature [1]. The tumor microvasculature is significantly more disorganized, tortuous and leaking

*Correspondence to: raimondo.penta@upm.es

(exhibiting large fenestrations) compared against its healthy counterpart. As a result, the normal circulation of blood and dispersed molecules may be compromised. Moreover, proliferating cancer cells alter the tumor microenvironment, collapsing blood and lymphatic vessels and destroying the physiological fluid flow [2]. Fluid accumulates in the interstitium, causing the interstitial fluid pressure to rise almost reaching the pressure level in the capillary network. Convective transport between the vascular and interstitial compartments - mainly driven by the transvascular pressure jump - is thus dramatically hindered, reducing mass exchange between the tumor and the vessels [3]. Therefore, malignant vascularization acts as an effective barrier, compromising the fluid transport and the delivery of therapeutic agents in the tumor [4], [5]. Relevant Experimental work (see, e.g. [6]), as well as mathematical models concerning tumor-induced angiogenesis (see, e.g. the review work [7]) and transport and consumption of drugs (see, e.g. [8]) can play a key role in elucidating the complex mechanisms and determinants underlying these phenomena and may contribute to the development of anti-cancer therapies. The aim of this work is to analyze the dependence of drug transport (in terms of advection, diffusion, and reaction) on the geometrical and physiological features of the tumor microvasculature. We start from the model presented in [9], where the authors apply asymptotic (periodic) homogenization [10] to derive a double Darcy, double advection-diffusion-reaction model describing the fluid and drug dynamics on the tissue scale. Balance equations for the fluid are upscaled starting from Darcy's law and the Stokes problem in the tumor interstitium and the capillary network, respectively. The dynamics and space distribution of a generic drug are formally described by an advection-diffusion model in both compartments, and possible drug uptake mechanisms are considered explicitly in the tumor interstitium. The mass and drug exchange through the capillary membrane is addressed via the non equilibrium thermodynamical model originally due to [11] and then developed in [12] and depends on the pressures and concentrations jumps across the vessels walls. These contributions translate into effective mass sources and reaction terms on the macroscale. The asymptotic homogenization upscaling process leads to a computationally feasible model, which can be solved on a coarse grid as only macroscale variations are to be resolved. However, the information concerning the microscale is encoded in the model coefficients, namely, the effective conductivities and diffusivities. These coefficients are to be computed solving classical differential problems on a periodic representative cell. In [13], the authors solve the fluid transport model developed in [14] (which can be derived as a particular case of [9] for negligible diffusion), computing the effective hydraulic conductivities for a number of prototypical geometries at increasing tortuosity. They deduce that geometrical tortuosity leads to impaired blood (and hence drug) advection within the tumor mass. Here, we extend their work by solving for the first time the multiscale model derived in [9] (under a number of simplifying assumptions) for different anti-cancer molecules and drug fluxes across the capillary walls. We recover the macroscale diffusivity tensors by solving Laplace-type cell problems at increasing vascular tortuosity. We track the macroscale drug concentration profile accounting for the effects of microvascular tortuosity on molecule diffusivity and uptake within the tumor mass.

The remainder of this work, which is intended to be the full-length version of the results briefly presented in [15], is organized as follows:

- In Section 2 we summarize the homogenized mathematical model [9], which is the starting point of the present analysis.

Prepared using cnmauth.cls
DOI: 10.1002/cnm

- In Section 3, we describe the microscale and macroscale computational approach embraced in this work and the report the cell problems' solution, as well as the appropriate physiological parameters taken (or estimated) from the experimental literature.
- In Section 4, we present the macroscopic model results and discuss the effects of microvascular tortuosity on drug transport in the tumor. We apply our mathematical framework to three different therapeutic agents and report on the model outcomes in terms of interstitial drug concentration and amount of metabolized drug.
- Finally, in Section 5 we present concluding remarks and further perspectives.

2. MATHEMATICAL MODELING

In [9], the authors extend the multiscale analysis presented in [14] to describe the interplay between the fluid and drug dynamics in vascularized tumors via a coupled double Darcy, double advection-diffusion-reaction system of PDEs at the tissue scale. On the local scale (identified by the intercapillary distance), the network of blood vessels and the tumor interstitium are considered as individual regions. Fluid transport is described by the Stokes' and Darcy's governing equations in the interstitial and capillary network compartments, respectively. Drug transport is governed by advection and diffusion of macromolecules in both compartments, together with possible consumption mechanisms in the tumor interstitium. Blood and drug exchange across the capillary walls is addressed via continuity of the corresponding fluxes, which are prescribed according to a fully non-equilibrium thermodynamical approach [11]. Blood flux is proportional to the hydrostatic pressure drop and to the osmotic pressure difference (due to the difference in drug concentrations), while drug flux comprises both a convective contribution (proportional to the blood flux), and a diffusive one related to the drug concentration jump. The multiscale homogenization approach carried out in [9] relies on the sharp scales separation between the intercapillary distance d ($\approx 50\mu$m) and the tumor size L under consideration ($\approx$ 1cm). According to [9], we then denote by ϵ the ratio between the two scales, i.e.

$$\epsilon = \frac{d}{L} \lll 1 \tag{1}$$

and we define two formally independent spatial variables $\boldsymbol{y}$ and $\boldsymbol{x}$ related by:

$$\boldsymbol{y} = \frac{\boldsymbol{x}}{\epsilon} \tag{2}$$

spanning the microscale and macroscale, respectively. We further enforce $\boldsymbol{y}$-periodicity and identify the microstructure with a periodic cell Ω and its interstitial and capillary portions by Ω_t and Ω_n, respectively, see Fig. 1. Enforcing asymptotic homogenization (see, e.g. [16, 17, 10]), we represent every field in terms of the two independent spatial variables defined in Equation (2) and express the solution in power series of the parameter ϵ. The upscaling process then provides a closed system of PDEs at the macroscale for the leading order components of the relevant fields, and represents the homogenized solution for vanishing ϵ. The geometric information at the microscale is not lost, as it is encoded in the arising effective hydraulic conductivity and diffusivity tensors. These auxiliary quantities are to be computed solving classical differential problems defined locally on a representative periodic cell. The final set of homogenized equations describes both the fluid

Prepared using cnmauth.cls
DOI: 10.1002/cnm

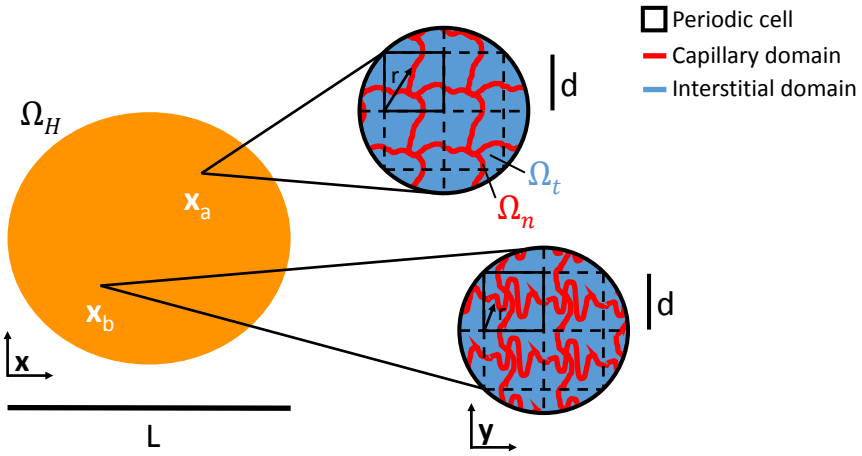

Figure 1. A 2D sketch of the microscale (right) vs the macroscale (left). On the macroscale, characterized by the homogenized domain Ω_H, the microscopic variations are smoothed out; on the microscale, the difference between the interstitial (Ω_t) and capillary (Ω_n) compartments in the periodic cell is highlighted. The microstructure is only locally periodic, and can vary over the macroscale.

and the drug dynamics in the tumor interstitium and vascular network at the tissue scale, while local fluid and drug exchange across the capillary walls translates into effective mass and reaction terms at the tissue scale.

In this work we aim at determining the impact of geometrical complexity on macromolecules diffusion, and how macroscopic diffusion affects, in turn, drug delivery and consumption in the tumor mass. Here we enforce the geometrical setup implemented in [13] for the blood transport problem, where a parametric analysis at varying tortuosity for a single periodic cell is performed. Therefore, we consistently specialize the non-dimensional tissue scale system of PDEs derived in [9] to the specific case of *macroscopic uniformity*, i.e. we neglect macroscopic variations of the microstructure. In the reminder of this work, we use the same notation convention reported in [9], denoting scalar, vectorial, and second rank tensorial quantities via different fonts, i.e. a, $\boldsymbol{a}$, and A (with components A_{ij}), respectively, for the sake of clarity. The subscripts n and t stand for the capillary network and the interstitial compartment, respectively.

Thus, the governing equations for the fluid transport problem read

$$\nabla_{\boldsymbol{x}} \cdot (\mathsf{K} \nabla_{\boldsymbol{x}} p_n) = \frac{S}{|\Omega_n|} \bar{\Phi}_b \tag{3}$$

$$\nabla_{\boldsymbol{x}} \cdot (\bar{\kappa} \mathsf{E} \nabla_{\boldsymbol{x}} p_t) = -\frac{S}{|\Omega_t|} \bar{\Phi}_b, \tag{4}$$

whereas for transport of macromolecules, assuming a linearized interstitial uptake rate:

$$\partial_t c_n + \nabla_{\boldsymbol{x}} \cdot (c_n \langle \boldsymbol{u}_n \rangle_n - \mathsf{D}_n \nabla_{\boldsymbol{x}} c_n) = -\frac{S}{|\Omega_n|} \bar{\Phi}_d \tag{5}$$

$$\partial_t c_t + \nabla_{\boldsymbol{x}} \cdot (c_t \langle \boldsymbol{u}_t \rangle_t - \mathsf{D}_t \nabla_{\boldsymbol{x}} c_t) = \frac{S}{|\Omega_t|} \bar{\Phi}_d - \overline{\mathrm{Da}}\, c_t \tag{6}$$

DOI: 10.1002/cnm

where Darcy's velocities are given by:

$$\langle \boldsymbol{u}_n \rangle_n = -\mathsf{K}\nabla_{\boldsymbol{x}} p_n \tag{7}$$

$$\langle \boldsymbol{u}_t \rangle_t = -\bar{\kappa}\mathsf{E}\nabla_{\boldsymbol{x}} p_t, \tag{8}$$

Here p_n and p_t are the leading macroscopic capillary and interstitial pressure fields, respectively, and c_n and c_t are the corresponding leading drug concentrations. The two velocities $\boldsymbol{u}_n$ and $\boldsymbol{u}_t$ are the leading order average Darcy velocities (with non-dimensional hydraulic conductivities K and $\bar{\kappa}\mathsf{E}$) describing fluid flow at the tissue scale. Note that Equations (3)-(8) are meant to be solved for every $\boldsymbol{x}$ in the macroscopic homogenized domain Ω_H. The reaction terms $\bar{\Phi}_b$ and $\bar{\Phi}_d$ appearing on the right hand side of Equations (3)-(6) represent blood and drug fluxes, respectively. When a complete Kedem-Katchalsky formulation is assumed [11], the resulting non-dimensional fluxes read:

$$\bar{\Phi}_b = \bar{L}_p \left(p_n - p_t\right) - \bar{\Pi}\left(c_n - c_t\right) \tag{9}$$

$$\bar{\Phi}_d = \left(1-\sigma\right) c_m \bar{\Phi}_b + \bar{\Upsilon}\left(c_n - c_t\right) \tag{10}$$

Here σ is the osmotic reflection coefficient ($0 < \sigma < 1$). This parameter quantifies the departure of a membrane behavior from semipermeability, being unitary for an ideal semipermeable membrane and zero for an unselective membrane. In general, the value of σ depends on the solute being considered and on the relative size of molecules and pores radii. Also, c_m denotes an average measure of the concentration within capillary walls. In [18] it is suggested to be a nonlinear function of the fluid flux:

$$c_m = (1-f)c_n + f c_t, \quad f = \frac{1}{\gamma\Phi_b} - \frac{1}{\exp\left(\gamma\Phi_b\right) - 1}, \quad \gamma = \frac{1-\sigma}{P} \tag{11}$$

Here $\gamma\Phi_b$ is the transvascular Péclét number (Pe) and expresses the relative importance of convection with respect to diffusion across the capillary surface. For suitable values of Pe the expression in Equation (11) can be linearized as:

$$\text{Pe} \ggg 1: \quad \bar{\Phi}_d = \left(1-\sigma\right) c_n \bar{\Phi}_b + \bar{\Upsilon}\left(c_n - c_t\right) \tag{12}$$

$$\text{Pe} \lll 1: \quad \bar{\Phi}_d = \left(1-\sigma\right) \bar{c}\, \bar{\Phi}_b + \bar{\Upsilon}\left(c_n - c_t\right), \quad \bar{c} = \frac{1}{2}\left(c_n + c_t\right) \tag{13}$$

An estimate of Pe for our system will be given in the next sections, together with the corresponding form for the drug flux. The non-dimensional numbers $\bar{L}_p$, $\bar{\kappa}$, $\bar{\Upsilon}$ and $\overline{\text{Da}}$ are the hydraulic permeability of the vessel walls, the interstitial conductivity, the diffusive permeability of the capillary membrane and the Damköhler number, respectively; $\bar{\Pi}$ measures the relative importance of osmotic and fluid pressure drop across the vessel wall. These quantities are defined by the following non-dimensional numbers:

$$\bar{L}_p = \frac{L_p L^2 \mu}{d^3}, \quad \bar{\Pi} = \frac{L_p L \mu \sigma R T C_r}{C d^3}, \quad \bar{\kappa} = \frac{k\mu}{d^2}, \quad \bar{\Upsilon} = \frac{P\mu L}{C d^3}, \quad \overline{\text{Da}} = \frac{\lambda L \mu}{C d^2} \tag{14}$$

where L_p is the hydraulic conductivity of the vessel walls and μ is the effective viscosity of blood. Note that here we are assuming a constant value for the latter parameter, neglecting the actual

DOI: 10.1002/cnm

non-Newtonian nature of blood for the sake of simplicity. Then, R is the universal gas constant, T is the absolute temperature, C_r and C are a reference drug concentration and pressure gradient, respectively. Finally, k is the hydraulic conductivity of the tissue, P is the diffusive permeability of the vessel walls and λ is the uptake rate in the interstitium. The representative cell exchange surface area S and volumes $|\Omega_n|$, $|\Omega_t|$ are defined by:

$$|\Omega_\alpha| = \int_{\Omega_\alpha} d\boldsymbol{y}, \alpha = n, t; \qquad S = \int_\Gamma dS_y \tag{15}$$

The conductivity tensors K and E are defined by:

$$\mathsf{K} = \langle \mathsf{W} \rangle_n, \quad \mathsf{E} = \mathsf{I} - \langle (\nabla_y \boldsymbol{P}_t)^\mathsf{T} \rangle_t \tag{16}$$

where I denotes the second order identity tensor and the brackets $\langle \cdot \rangle_\alpha$ stand for the cell average operator:

$$\langle \cdot \rangle_\alpha = \frac{1}{|\Omega_\alpha|} \int_{\Omega_\alpha} \cdot \, d\boldsymbol{y}, \quad \alpha = n, t \tag{17}$$

The auxiliary tensors $\mathsf{W}(\boldsymbol{y})$ and $\boldsymbol{P}_t(\boldsymbol{y})$ satisfy the following *cell problems*:

$$\nabla_y^2 \mathsf{W}^\mathsf{T} - \nabla_y \boldsymbol{P}_n + \mathsf{I} = 0 \quad \text{in } \Omega_n \tag{18}$$

$$\nabla_y \cdot \mathsf{W}^\mathsf{T} = 0 \quad \text{in } \Omega_n \tag{19}$$

$$\mathsf{W}^\mathsf{T} \boldsymbol{n} = 0 \quad \text{on } \Gamma \tag{20}$$

$$\mathsf{W}^\mathsf{T} \boldsymbol{\tau} = 0 \quad \text{on } \Gamma \tag{21}$$

$$\nabla_y^2 \boldsymbol{P}_t = 0 \quad \text{in } \Omega_t \tag{22}$$

$$(\nabla_y \boldsymbol{P}_t)\, \boldsymbol{n} = \boldsymbol{n} \quad \text{on } \Gamma \tag{23}$$

where the auxiliary quantities $\boldsymbol{P}_n$ and $\boldsymbol{P}_t$ fulfill the uniqueness conditions:

$$\langle \boldsymbol{P}_n \rangle_n = 0 \quad \text{in } \Omega_n \qquad \text{and} \qquad \langle \boldsymbol{P}_t \rangle_t = 0 \quad \text{in } \Omega_t \tag{24}$$

The other two tensors D_n and D_t in Equations (5)-(6) are the effective diffusivities for the capillary and interstitial compartments, respectively. They are given by the formula:

$$\mathsf{D}_n = A_n \left(\mathsf{I} - \langle (\nabla_y \boldsymbol{a})^\mathsf{T} \rangle_n \right), \quad \mathsf{D}_t = A_t \left(\mathsf{I} - \langle (\nabla_y \boldsymbol{b})^\mathsf{T} \rangle_t \right) \tag{25}$$

where A_n and A_t are the non-dimensional diffusivities for the two compartments:

$$A_n = \frac{D_n \mu}{LCd^2}, \quad A_t = \frac{D_t \mu}{LCd^2} \tag{26}$$

DOI: 10.1002/cnm

and D_n, D_t are their dimensional counterparts. The auxiliary vectors $\boldsymbol{a}$ and $\boldsymbol{b}$ satisfy the cell problems:

$$\nabla_y^2 \boldsymbol{a} = 0 \quad \text{in } \Omega_n \tag{27}$$

$$(\nabla_y \boldsymbol{a})\, \boldsymbol{n} = \boldsymbol{n} \quad \text{on } \Gamma \tag{28}$$

$$\nabla_y^2 \boldsymbol{b} = 0 \quad \text{in } \Omega_t \tag{29}$$

$$(\nabla_y \boldsymbol{b})\, \boldsymbol{n} = \boldsymbol{n} \quad \text{on } \Gamma \tag{30}$$

where, again, a further condition on $\boldsymbol{a}$ and $\boldsymbol{b}$ for their uniqueness is required, namely:

$$\langle \boldsymbol{a} \rangle_n = 0 \quad \text{in } \Omega_n, \qquad \langle \boldsymbol{b} \rangle_t = 0 \quad \text{in } \Omega_t \tag{31}$$

Exploiting periodicity in the $\boldsymbol{y}$-variable, the cell problems for the previous tensor quantities are closed by periodic conditions on the cell boundaries $\Omega_n \setminus \Gamma$ and $\Omega_t \setminus \Gamma$ for the corresponding compartments. Note that the cell problems are actually classical differential problems, since Equations (18)-(21) is a Stokes' type boundary value problem and Equations (22)-(23),(27)-(28),(29)-(30) are inhomogeneous Laplace problems.

In the next section we provide a detailed description of the computational setup and physiological parameters that we have exploited to solve the microscale periodic cell problems and, in turn the fluid and drug transport problem on the tissue scale. We start illustrating (a) a suitable algorithm to obtain the solution of the problem in a few simple steps for macroscopically uniform structures, (b) the physiological parameters exploited in the computations, (c) the microscale cell problem computational setup for a tortuous microvasculature, (d) the macroscale problem for a spherical, tissue scale tumor geometry.

3. MICROSCALE AND MACROSCALE COMPUTATIONAL SETUP

The computational steps needed to calculate the solution of the macroscale problem (3)-(8) can be summarized as follows

- Given a time interval $(0, T)$ and the macroscale spatial domain Ω_H, fix suitable initial and boundary conditions.
- Set the model parameters and calculate the non-dimensional numbers in Equation (14)
- Set the representative cell and compute the geometrical parameters $|\Omega_n|$, $|\Omega_t|$ and S.
- Solve the cell problems (18)-(24) and (27)-(31) to find the auxiliary quantities $\mathsf{W}, \boldsymbol{P}_t, \boldsymbol{P}_n, \boldsymbol{a}$ and $\boldsymbol{b}$.
- Compute the effective conductivities and diffusivities $\mathsf{K}, \mathsf{E}, \mathsf{D}_n$ and D_t using Equations (16) and (25).
- Solve the differential problem in Equations (3)-(8) supplemented by the initial and boundary conditions given in the first step.

Prepared using cnmauth.cls
DOI: 10.1002/cnm

We emphasize that the mathematical model is to be solved on the homogenized domain Ω_H, nonetheless retaining all the relevant physical phenomena in the effective coefficients. A numerical solution of the original problem would require an extremely refined spatial discretization to capture all the details of the microstructure. However, since the effective governing Equations (3)-(6) are defined on the macroscale domain, a significantly coarser grid can be used. The geometric features of the microscale are now encoded into four constant symmetric positive definite tensors, namely the capillary and interstitial effective hydraulic conductivities and diffusivities. As a first step, we assume *macroscopic uniformity*, as in [13], such that the periodic auxiliary quantities are computed over a single periodic cell only once for every point $\boldsymbol{x} \in \Omega_H$ (see Figure 1), via the solution of Stokes' and Laplace's differential problems. For a discussion concerning non-macroscopic uniformity and the subsequent increase in computational complexity, see, e.g. [17] and [19], respectively.

3.1. Physiological parameters

The parameters used in the simulations are collected in Table I and Table II. It was not possible

Table I. Parameters characterizing the fluid and drug transport problem.

Symbol	Parameter	Unit	Value	Reference
L_p	Vessel hydraulic permeability	$\mathrm{m}/(\mathrm{Pa\ s})$	1.78×10^{-11}	[20]
k	Tumor hydraulic conductivity	$\mathrm{m}^2/(\mathrm{Pa\ s})$	2.1×10^{-13}	[21]
μ	Blood viscosity	Pa s	4.0×10^{-3}	[22]
d	Reference microscale	m	4.0×10^{-5}	[23]
L	Reference macroscale	m	1.0×10^{-2}	[24, 20]
C	Reference pressure gradient	Pa/m	5×10^2	[13, 14]
R	Tumor radius	m	5.0×10^{-3}	[24, 20]
T	Time interval	h	96	-
P	Vessel wall permeability (ref. drug)	m/s	1.7×10^{-7}	[25, 26]
D_n	Diffusivity in the capillaries (ref. drug)	m^2/s	3.3×10^{-10}	[14]
D_t	Diffusivity in the interstitium (ref. drug)	m^2/s	1.0×10^{-11}	[14]
λ	Uptake in the interstitium (ref. drug)	$1/\mathrm{s}$	1.07×10^{-11}	[14]
τ	Plasma clearance time constant (ref. drug)	h	6	[27]

Table II. Parameters for the two representative drugs.

Symbol	Parameter	Unit	Value	Reference
D_n^{vin}	Capillary diffusivity (Vinblastine)	m^2/s	3.3×10^{-10}	[14]
D_t^{vin}	Interstitial diffusivity (Vinblastine)	m^2/s	1.9×10^{-12}	[14]
P^{vin}	Vessel wall permeability (Vinblastine)	m/s	1.2×10^{-6}	[14]
τ^{vin}	Plasma clearance time constant (Vinblastine)	h	25	[28]
λ^{vin}	Uptake in the interstitium (Vinblastine)	$1/\mathrm{s}$	1.07×10^{-11}	[14]
D_n^{dox}	Capillary diffusivity (Doxorubicin)	m^2/s	4.8×10^{-10}	[29]
D_t^{dox}	Interstitial diffusivity (Doxorubicin)	m^2/s	5.01×10^{-11}	[30]
P^{dox}	Vessel wall permeability (Doxorubicin)	m/s	1.95×10^{-6}	[31]
τ^{dox}	Plasma clearance time constant (Doxorubicin)	h	22.5	[32, 33]
λ^{dox}	Uptake in the interstitium (Doxorubicin)	$1/\mathrm{s}$	5.8×10^{-5}	[30]

to find in the literature an estimate for two parameters, namely the reflection coefficient σ and the transvascular Péclét number Pe. Regarding the first, we follow the work in [34, chap. 7], where σ is

DOI: 10.1002/cnm

calculated from the mathematical expression:

$$\sigma = \frac{16}{3}\alpha^2 - \frac{20}{3}\alpha^3 + \frac{7}{3}\alpha^4, \quad \alpha = \frac{r_{\text{mol}}}{r_{\text{por}}} \tag{32}$$

and the constant α is given by the ratio between the molecule and the pore radii in the capillary membrane. According to the observations in [20], we estimate $r_{\text{por}} = 1.0\mu$m, a value consistent with the multiple fenestrations that characterize a malignant vascular network. The molecule radius can be estimated from the Stokes-Einstein equation:

$$r_{\text{mol}} = \frac{k_B T}{6\pi\mu D_{\text{mol}}} \tag{33}$$

where $k_B T$ is the Boltzmann thermal energy. We find $r_{\text{vin}} = 2.98 \times 10^{-8}$m and $r_{\text{dox}} = 1.13 \times 10^{-9}$m for Vinblastine and Doxorubicin radii, respectively. Using these estimates for the radii, we obtain the values $\sigma_{\text{vin}} = 4.56 \times 10^{-3}$ and $\sigma_{\text{dox}} = 6.8 \times 10^{-6}$ via Equation (32). The value of the transvascular Péclét number can be obtained from the relation in Section 2, assuming:

$$\text{Pe} = \gamma\Phi_b = \left(\frac{1-\sigma}{P}\right)(L_p \Delta p) \tag{34}$$

where Δp is a suitable value for the pressure difference between the capillary and interstitial compartments. According to [20], we take $\Delta p \approx 10^3$ Pa and obtain the estimate $\text{Pe} \approx 10^{-2}$ using the numbers in Tables I and II. This value suggests to consider the linear regime proposed in Equation (13) for the drug flux $\bar{\Phi}_d$, indicating that drug exchange is mainly due to diffusion across the capillary membrane for this kind of molecules.

From the parameters in table I and II it is also possible to provide an estimate for the value of the non-dimensional number $\bar{\Pi}$ in Equation (14). Using the highest value for σ, we find:

$$\bar{\Pi} = \frac{L_p L \mu \sigma R T C_r}{C d^3} \simeq 0.05 \frac{\ell}{\text{mol}} \times C_r \tag{35}$$

Since a realistic value for the reference concentration of the drugs that we considered is given by $C_r \simeq 1 \div 10 \times 10^{-6}\,\text{mol}/\ell$ [35, 36], we obtain the estimate $\bar{\Pi} \simeq 5 \div 50 \times 10^{-8}$. We can thus simplify the expression for the fluid flux in Equation (10), which now reads:

$$\bar{\Phi}_b = \bar{L}_p\,(p_n - p_t) \tag{36}$$

$$\bar{\Phi}_d = (1-\sigma)\,\bar{c}\,\bar{\Phi}_b + \bar{\Upsilon}\,(c_n - c_t) \tag{37}$$

where we have also reported the updated expression for the drug flux.

3.2. Periodic cell problems' solution for a tortuous microvasculature

In [13], the cell problems related to the hydraulic conductivity tensors K and E are discussed in detail. The authors evaluate the influence of the blood vessels' tortuosity on fluid transport in the tumor tissue. In particular, they consider different unit cells varying the vessels' tortuosity and track the changes in hydraulic conductivities of the capillary and interstitial compartments. This way, they qualitatively and quantitatively describe the hampering effect of vascular geometrical complexity

Prepared using cnmauth.cls
DOI: 10.1002/cnm

on fluid convection. Following this approach, here we focus on the solution of the cell problems for the effective diffusivities D_n and D_t given by (27-28) and (29-30), respectively. Each of the latter vectorial Laplace problems, which are in terms of $\mathbf{a}$ and $\mathbf{b}$, is equivalent to three standard scalar Laplace problems for the components a_1, a_2, a_3 and b_1, b_2, b_3, respectively. According to the analysis reported in [13], we note that an isotropic problem for the concentrations at the macroscale can be obtained if the effective diffusivity tensors satisfy the relations:

$$\mathsf{D}_n = \tilde{D}_n \mathsf{I}, \quad \mathsf{D}_t = \tilde{D}_t \mathsf{I} \tag{38}$$

with $\tilde{D}_n$ and $\tilde{D}_t$ given by:

$$\tilde{D}_n = A_n \left(1 - \langle \frac{\partial a_1}{\partial y_1} \rangle_n \right) = A_n \left(1 - \langle \frac{\partial a_2}{\partial y_2} \rangle_n \right) = A_n \left(1 - \langle \frac{\partial a_3}{\partial y_3} \rangle_n \right) \tag{39}$$

$$\tilde{D}_t = A_t \left(1 - \langle \frac{\partial a_1}{\partial y_1} \rangle \right) = A_t \left(1 - \langle \frac{\partial a_2}{\partial y_2} \rangle_n \right) = A_t \left(1 - \langle \frac{\partial a_3}{\partial y_3} \rangle_n \right) \tag{40}$$

In order to satisfy the isotropic representations reported above, we select the same microstructures exploited in [13], which are characterized by three orthogonal branches and invariance under permutations of the three coordinate axes. The latter feature leads to the following componentwise relationships

$$\frac{\partial a_3}{\partial y_1} = \frac{\partial a_1}{\partial y_2} = \frac{\partial a_2}{\partial y_3}, \qquad \frac{\partial b_3}{\partial y_1} = \frac{\partial b_1}{\partial y_2} = \frac{\partial b_2}{\partial y_3} \tag{41}$$

$$\frac{\partial a_3}{\partial y_2} = \frac{\partial a_1}{\partial y_3} = \frac{\partial a_2}{\partial y_1}, \qquad \frac{\partial b_3}{\partial y_2} = \frac{\partial b_1}{\partial y_3} = \frac{\partial b_2}{\partial y_1} \tag{42}$$

$$\frac{\partial a_3}{\partial y_3} = \frac{\partial a_1}{\partial y_1} = \frac{\partial a_2}{\partial y_2}, \qquad \frac{\partial b_3}{\partial y_3} = \frac{\partial b_1}{\partial y_1} = \frac{\partial b_2}{\partial y_2}. \tag{43}$$

Hence, we only need to solve two scalar Laplace's problems, for example in terms of a_3 and b_3 as reported below.

$$\nabla_y^2 a_3 = 0 \quad \text{in } \Omega_n \tag{44}$$

$$\nabla_y a_3 \cdot \boldsymbol{n} = n_3 \quad \text{on } \Gamma \tag{45}$$

$$\nabla_y^2 b_3 = 0 \quad \text{in } \Omega_t \tag{46}$$

$$\nabla_y b_3 \cdot \boldsymbol{n} = n_3 \quad \text{on } \Gamma \tag{47}$$

$$\langle a_3 \rangle_n = 0 \quad \text{in } \Omega_n, \qquad \langle b_3 \rangle_t = 0 \quad \text{in } \Omega_t. \tag{48}$$

We then recover the full solution for D_n and D_t through the definitions in Equation (25) and exploiting relationships (41). As expected from the analysis of the Stokes' probles reported in [13], the chosen microstructure geometry reflects in negligible extra-diagonal components, when compared to the diagonal ones. We therefore account for the isotropic representations (39) and (40) for the purpose of our analysis. As done in [13] for the hydraulic conductivity, the impact of tortuosity is tested on the effective diffusivities by varying the geometrical configurations of Ω_n and

DOI: 10.1002/cnm

Ω_t. We introduce two parameters, A and ω, that lead to different tortuosity in the vascular network through an analytical parametrization of the capillary centerline. The representative capillary network cell portion is shown in Figure 2. The capillary and interstitial cell problems are solved

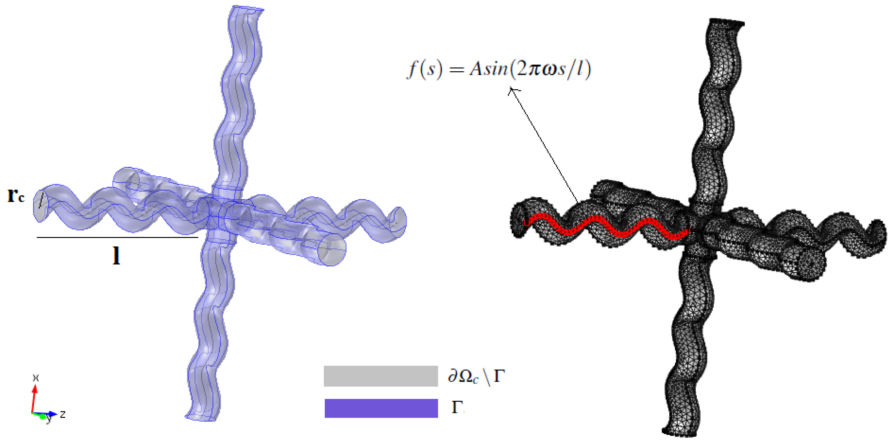

Figure 2. An example of the tortuous capillary network cell portion is shown on the left. The paramters l and r_c are the one-sided branch length and capillary radius, respectively, [13]. The corresponding three-dimensional mesh and the analytical parametrization of the capillary centerline is shown on the right. Reprinted from The Journal of Theoretical Biology, Volume 364, The role of microvascular tortuosity in tumor transport phenomena, Pages No. 80-97, Copyright (2015), with permission from Elsevier.

via the commercial finite element software COMSOL Multiphysics, where Equations (44)-(48) are discretized by standard $\mathbb{P}_2$ elements. By selecting different values of the tortuosity parameters A and ω we vary the geometrical tortuosity of the representative cell and then we compute the values of the effective diffusivities D_n and D_t. Results are presented in Table III, where we report the values of the effective diffusivities for geometries with different tortuosity, together with the corresponding values for S, $|\Omega_n|$ and $|\Omega_t|$. Comparison between the two extreme tortuosity regimes (from now

Table III. Computational results for the non-dimensional capillary and interstitial diffusivities D_n and D_t, cell exchange surface S and capillary and interstitial cell volume portions $|\Omega_n|$ and $|\Omega_t|$. With reference to Figure 2, three geometries with varying tortuosity are tested, parametrized by different values of ω.

ω	A	$\tilde{D}_n/A_n$	$\tilde{D}_t/A_t$	S	$\lvert\Omega_n\rvert$	$\lvert\Omega_t\rvert$
0	0	3.6×10^{-1}	1	2.30	8.1×10^{-2}	6.149
1	$0.25r_c$	3.57×10^{-1}	1	2.30	8.0×10^{-2}	6.15
1	$0.5r_c$	3.53×10^{-1}	1	2.30	7.9×10^{-2}	6.151
1	$0.75r_c$	3.4×10^{-1}	1	2.31	7.8×10^{-2}	6.152
1	r_c	3.19×10^{-1}	1	2.32	7.6×10^{-2}	6.154
2	$0.25r_c$	3.54×10^{-1}	1	2.30	7.9×10^{-2}	6.151
2	$0.5r_c$	3.18×10^{-1}	1	2.33	7.6×10^{-2}	6.154
2	$0.75r_c$	2.65×10^{-1}	1	2.42	7.2×10^{-2}	6.158
2	r_c	2.13×10^{-1}	1	2.57	6.9×10^{-2}	6.161
3	$0.25r_c$	3.37×10^{-1}	1	2.32	7.8×10^{-2}	6.152
3	$0.5r_c$	2.47×10^{-1}	1	2.53	7.2×10^{-2}	6.158
3	$0.75r_c$	1.59×10^{-1}	1	2.82	6.8×10^{-2}	6.162
3	r_c	0.9×10^{-1}	1	3.25	6.5×10^{-2}	6.165

on named “Regular” and “Tortuous”) shows that, even for a regular microvasculare, there exists an almost 3-fold drop in capillary effective diffusivity with respect to the base value. For the tortuous

Prepared using cnmauth.cls
DOI: 10.1002/cnm

case, we observe an up to 10-fold decrease. Concerning the interstitium, we note that the effective diffusivity is not affected by the variation of geometry. This is consistent with the results in [13], where a similar behavior is observed for the effective hydraulic conductivity E (which is likewise computed via problem (46-47) and it is indeed equivalent to $\frac{1}{A_t}\mathsf{D}_t$) as long as $|\Omega_n| \ll |\Omega|$, where $|\Omega| = |\Omega_n| + |\Omega_t|$.

3.3. Macroscale governing equations for a spherical tumor

We assume that the tissue scale tumor geometry can be represented by a sphere of radius R. The tumor is supposed to be isolated, consisting of a vascularized mass that interacts with the environment only through the substances transported by the microvasculature. The influence of an external stress or biochemical activity is neglected, and we focus mainly on the effect of vascular tortuosity on the transport of injected drugs. Enforcing radial symmetry, the Equations for the leading order drug concentrations (5)-(6) read:

$$\frac{\partial c_n}{\partial t} + \frac{1}{r^2}\frac{\partial}{\partial r}\left[r^2\left(u_n c_n - \tilde{D}_n \frac{\partial c_n}{\partial r}\right)\right] = -\frac{S}{|\Omega_n|}\bar{\Phi}_d \tag{49}$$

$$\frac{\partial c_t}{\partial t} + \frac{1}{r^2}\frac{\partial}{\partial r}\left[r^2\left(u_t c_t - \tilde{D}_t \frac{\partial c_t}{\partial r}\right)\right] = \frac{S}{|\Omega_t|}\bar{\Phi}_d - \overline{\mathrm{Da}}\, c_t \tag{50}$$

where each variable is a function of the radial coordinate r and of the time t. The latter is supposed to span the interval $(0, T)$, while r covers the tumor domain, namely $0 \leq r \leq R$. Here the radial components of the capillary and interstitial velocities u_n and u_t are given by solution of the fluid transport problems in [13], corresponding to Equations (3)-(4) and (7)-(8). We assume that drug capillary concentration drives drug evolution in the interstitium. This is imposed by selecting suitable boundary conditions. To this end, we model a bolus injection of drug in the tumor vessels by fixing the concentration in the capillaries at $r = R$. This concentration decreases exponentially with time according to the plasma clearance time constant τ (see [27]). Concerning the interstitial compartment, we assume that the drug does not diffuse into the outer tissue. Symmetry at the tumor center implies a null drug flux in $r = 0$. Finally, assuming that no drug is present at the beginning of the simulation in both compartments, the complete set of initial and boundary conditions is given by:

$$c_n\big|_{t=0} = c_t\big|_{t=0} = 0 \tag{51}$$

$$\left(u_n c_n - \tilde{D}_n \partial_r c_n\right)\big|_{r=0} = \left(u_t c_t - \tilde{D}_t \partial_r c_t\right)\big|_{r=0} = 0 \tag{52}$$

$$c_n\big|_{r=R} = \exp(-t/\tau), \quad -\tilde{D}_t \partial_r c_t\big|_{r=R} = 0. \tag{53}$$

The governing Equations of the macroscale model in (49)-(53) are discretized via the finite element program COMSOL Multiphysics. The spatial discretization is carried out via standard $\mathbb{P}_2$ elements, whereas for the discretization in time an implicit BDF method is used.

Prepared using cnmauth.cls
DOI: 10.1002/cnm

4. RESULTS AND DISCUSSION

We investigate the role of the geometrical properties of the microvasculature on the capillary diffusivity and consumption of an injected drug. We model the drug dynamics by means of the homogenized mathematical model illustrated in the previous sections, thus extending the previous work developed in [13]. In sections 4.1-3 we consider the simplified form of Equation (37) given by:

$$\bar{\Phi}_d = \bar{\Upsilon}\,(c_n - c_t) \tag{54}$$

where we neglect the convective contribution to the drug flux. The effect of the latter contribution (which in the experimental literature is usually encoded in the diffusive membrane permeability for the sake of convenience) on the drug distribution profiles will be evaluated separately in section 4.4. The results are presented in terms of the tumor drug concentration c_t (and related quantities) against the relative radius $\hat{r} = r/R$.

4.1. Effects of diffusion and uptake on drug distribution

The cell problems in (44)-(48) are solved in three dimensional space for different complexities of the microvascular geometries. The resulting diffusivity tensors are injected into the macroscale model (49)-(50) to track the evolution of drug concentration in the tumor. Results from the simulations corresponding to the parameters in Table I are displayed in Figure 3 and 4. We consider the dynamics of a generic drug, focusing on the effects of diffusion on drug transport. We report a

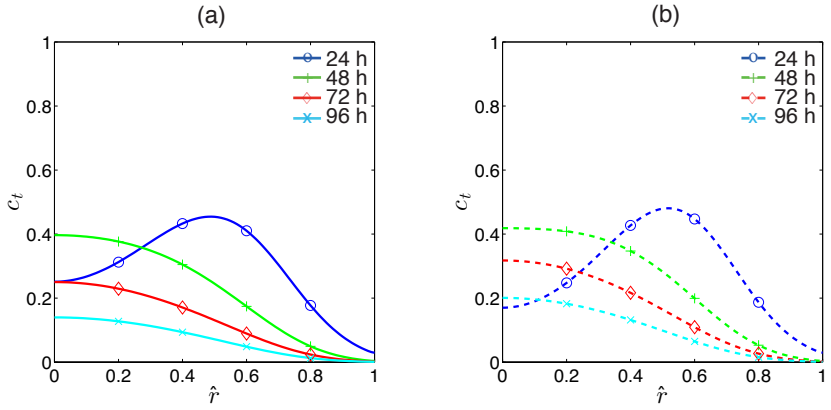

Figure 3. Regular microvasculature, drug distribution in the presence (solid lines) or absence (dashed lines) of the diffusion damping effect.

significant decrease in capillary diffusivity for increasing tortuosity of the microvascular network. Compared to the base value A_n, we observe a 3-fold drop in the case of a regular microvasculature and an up to 10-fold reduction in the most tortuous vascular network (see Table III). The decrease in molecule diffusivity can be observed comparing the solid and dashed lines in Figure 3.a and 3.b, where the drug interstitial concentration c_t is represented as a function of tumor relative radius $\hat{r}$ for different times. Both figures are determined for a regular microvasculature, but for the dashed lines the diffusivity tensors D_n and D_t are taken equal to the base values A_n and A_t, respectively. On the other hand, for the solid lines the two tensors are obtained solving the cell problems and

Prepared using cnmauth.cls
DOI: 10.1002/cnm

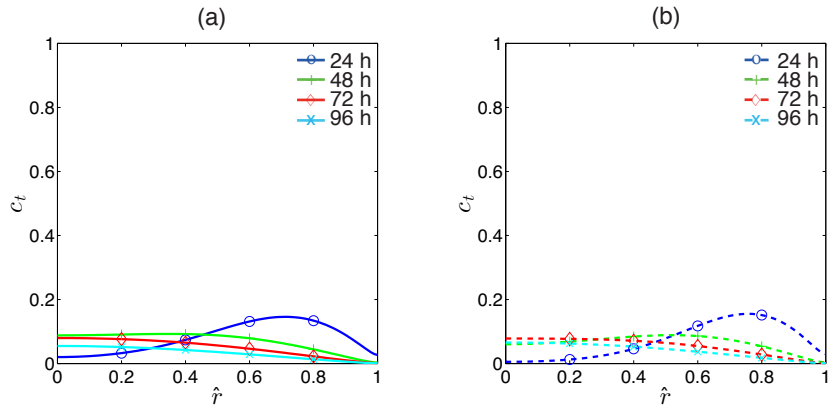

Figure 4. Tortuous microvasculature, drug distribution in the presence (solid lines) or absence (dashed lines) of the diffusion damping effect.

calculating the integrals in Equations (39)-(40). Note that even though the diffusivity is reduced, the molecule transport is not fully compromised. This is due to the regular microvasculature and the corresponding unimpaired hydraulic conductivity. Fluid convection is still functional and this enables the tumor interior to be reached by the drug after a certain time. The effect of network tortuosity is displayed clearly in Figure 4.a and 4.b, where the same comparison is carried out for a tortuous microvasculature. In this case both molecule diffusivity and advection are compromised, and also drug uptake proves significantly altered. In particular, a reduced effective diffusivity is responsible for a more compact drug distribution that travels towards the center of the tumor. This produces local values of c_t that are higher than their not-damped counterparts, as shown more clearly in Figure 2 of [15].

4.2. Analysis of two representative drugs

In this section the mathematical model is tested against two representative drugs, commonly found in the clinical literature. The first medication, Vinblastine, is an antimicrotubule drug generally used to treat a variety of cancers, including Hodgkin's lymphoma, non-small cell lung cancer, breast cancer, head and neck cancer, and testicular cancer [37]. Via binding with tubulin, the molecule inhibits assembly of microtubules and leads to cell death. The second molecule that we consider is Doxorubicin, a chemotherapeutic agent used to treat several cancers including blood cancers and many types of carcinoma [38]. The primary mechanism of action of Doxorubicin is DNA intercalation with the subsequent halting of the process of cell replication. The parameters used in the simulations are collected in Table II. Note that, despite some of the molecule parameters are very similar (e.g. the diffusion coefficients and the plasma clearance), the uptake rate of the molecules greatly differ between the two drugs. Vinblastine behaves like a tracer molecule, with a small absorption in the tissue, while the Doxorubicin uptake rate is several orders of magnitude higher. The evolution of Vinblastine interstitial concentration is shown in Figure 5 vs the radius of the tumor and for different times in the interval $(0 - 96h)$. In this case molecule distribution is strongly dictated by the fluid dynamics of the two compartments. According to the results reported in Figure 5.a for a regular microvasculature, the molecule is able to travel for a long distance into the tumor before being washed away from the system. At the end of the simulation, a small portion of

Prepared using cnmauth.cls
DOI: 10.1002/cnm

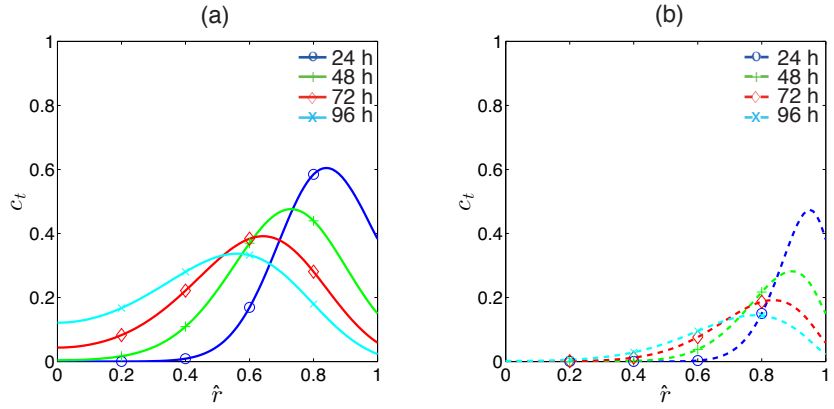

Figure 5. Vinblastine dynamics for a regular (a) and a tortuous (b) microvasculature.

the drug reaches the center of the tumor and interacts with the cancer cells. On the other hand, Figure 5.b shows the effect of a tortuous microvasculature on the drug dynamics. The radius reached by the molecule is considerably smaller when compared to the regular case (see 5.a) and after four days no drug is present in the tumor center. The geometrical complexity of the network is also responsible for the decrease in molecular diffusion. As a consequence, the drug concentration profile is more localized in space (see Figure 5) and this effect contributes in impairing drug transport in the internal portion of the tumor.

The case of Doxorubicin is dramatically different. This molecule interacts strongly with the interstitial compartment and its dynamic is dominated by tissue uptake. Figure 6 represents the interstitial concentration of Doxorubicin versus time and tumor radius. Here the effect of a regular

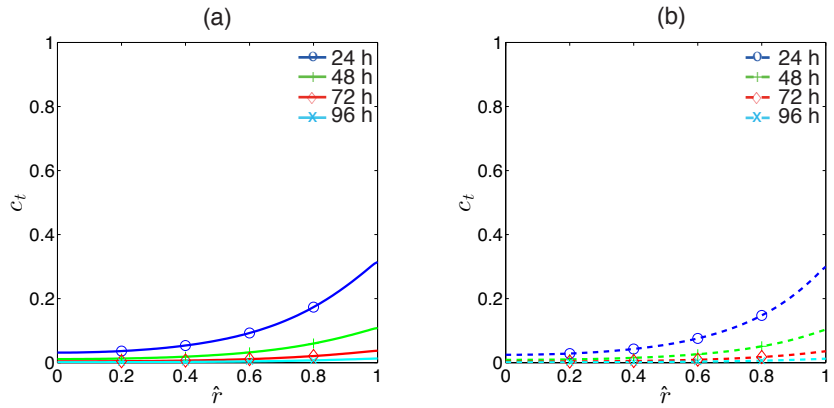

Figure 6. Doxorubicin dynamics for a regular (a) and a tortuous (b) microvasculature.

(6.a) or tortuous (6.b) microvasculature is less relevant for the evolution of the system. With reaction dominating the scene, the timescale of the phenomena is shifted towards shorter times. The effects of convection and diffusion, for which the complexity of the microvasculature plays a main role, operates at later times and the two dynamics do not overlap. As a result, the concentration profile is almost independent from the geometrical complexity of the vascular network, and the effectiveness of the drug has to be evaluated using different indexes (an example of which will be given in Section 4.3). Note that for a molecule of this kind a therapy focusing only on the improvement

Prepared using cnmauth.cls
DOI: 10.1002/cnm

of mass transport in the tumor may be inadequate, and additional measures should be undertaken to guarantee better drug efficacy.

4.3. Metabolized drug

From a clinical perspective, the interstitial concentration of a drug may not be a significant proxy for evaluating the treatment performance. In this section we introduce the auxiliary quantity $\mathsf{M}(r)$, to account for the quantity of drug metabolized in the tumor as a function of its radius. This quantity is defined as:

$$\mathsf{M}(r) = \int_0^T R\left[c_t(r,t')\right]\, dt' \tag{55}$$

where T is the time interval considered in the simulations and $R\left[\cdot\right]$ is the reaction term in Equation (6). For linear uptake, as the one considered in this work, the latter term reads:

$$\mathsf{M}(r) = \int_0^T \overline{\mathrm{Da}}\, c_t(r,t')\, dt' \tag{56}$$

with $\overline{\mathrm{Da}}$ being the Damköhler number calculated in Equation (14). In Figure 7 this quantity is plotted for the two molecules examined in the previous section. Figure 7.a shows the results for Vinblastine.

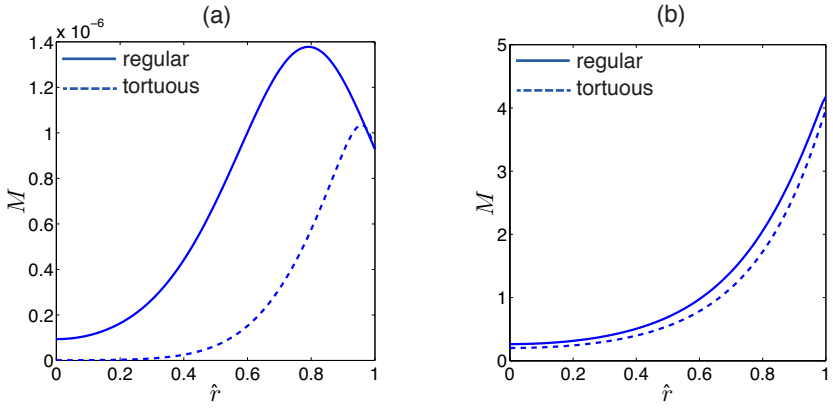

Figure 7. Metabolized drug for Vinblastine (a) and Doxorubicin (b). Solid lines refer to a regular microvasculature, dashed lines to a tortuous one.

Here the solid line indicates the case of a regular microvasculature, while the dashed line stands for the tortuous case. There is a marked difference between the two vascular regimes, both in terms of curve amplitudes and maxima locations. Regarding the first result, more drug is metabolized in a regular network, with a value different from zero also in the tumor center. The curve peak is shifted from the outer boundary of the tissue towards the tumor center, as fluid convection is still effective. Conversely, for a tortuous microvasculature the amount of metabolized drug is less and is delimited to the first half of the domain, near the tumor boundary. Diffusion and convection are hindered due to the geometrical complexity of the network, and at the end of the simulation a negligible quantity of drug is able to reach the cancer cells located in the tumor center.

The case of Doxorubicin is shown in Figure 7.b. Again, solid and dashed lines describe a regular and a tortuous microvasculature, respectively. For Doxorubicin, the maximum value of $M(r)$ is greater than the corresponding value for Vinblastine. This results from the high value of the

DOI: 10.1002/cnm

Damköhler number in this second molecule with respect to Vinblastine. The amount of metabolized drug decays almost exponentially from the border of the tumor towards its center, where the value is about 10% of the maximum. Even though the two curves are very similar, we note smaller values of $M(r)$ in the case of a tortuous microvasculature over all the tumor radius.

4.4. Convective contribution to the drug flux

In the previous sections we have only considered the diffusive contribution to the drug exchange across the capillary membrane. However, in general, we should also account for the convective contribution to the drug flux (cf. relationship (37)), which is proportional to the pressure difference between the two tissue compartments. However, the complete formulation for the drug flux is rarely implemented in the literature. The experimental measurement of the vessel diffusive permeability P is actually extremely complex, since it should account only for the diffusive portion of the drug flux, neglecting the convective counterpart. Thus, this second contribution to the flux is generally ignored in the modeling literature and an higher effective permeability P_{eff} is instead considered. In this Section we take into account the complete formulation (37) for the drug flux, and compare the results with the previously implemented approximation. The corresponding results are displayed in Figure 8 for a regular (8.a) and a tortuous (8.b) microvasculature. We use the parameters of

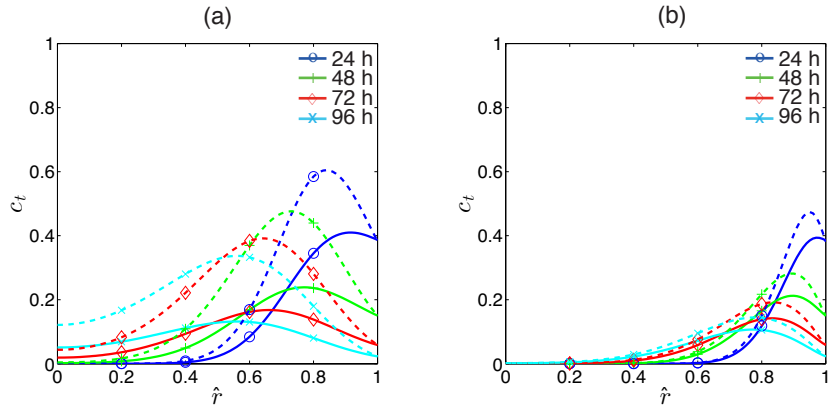

Figure 8. Comparison between the two drug fluxes Φ_d proposed in the model. The parameters are those of Vinblastine and a regular (a) and a tortuous microvasculature (b) are considered. The two cases with a complete drug flux or with a purely diffusive contribution are represented by solid or dotted lines respectively.

Vinblastine from Section 3.1. The evolution of the system is similar to the previous case in Figure 5, reported in Figure 8 with dotted lines. The qualitative dynamics of the system are similar to the case where we account for a diffusive contribution only. We observe an analogous concentration drop due to the hindered fluid flow in the tortuous network, combined with the same decrease in molecule diffusivity. The effects of the new term in Equation (37) become apparent when we compare the amplitude of the curves. The new drug flux law provides a lower concentration over the whole tumor domain and for each considered time interval. At a first glance these results seem counterintuitive, as we could expect that an increase in (fluid-driven) drug convection across the capillary walls should result in a corresponding increase of drug concentration in the tumor mass. A possible explanation of this phenomenon may be given recalling the experimental observations of Jain and coworkers on

DOI: 10.1002/cnm

the role of vessel permeability in tumor angiogenesis [27, 6, 20, 5]. Jain and his group carry out a series of experiments where they evaluate the permeability of capillary membranes in tumor vessels - a measure of L_p in our equations - and link this quantity with the fluid dynamics in the tumors. They observe that even though tumor vessels are characterized by high permeabilities, the exchange of fluids and solutes across vessel membranes is markedly hampered. This occurs as the pressure gradients between capillaries and interstitium cancel out due to the altered fluid exchange, and the corresponding fluid flow vanishes. Moreover, since the lymphatic system in the tumor is usually not functional, the fluid stagnates in the interstitium and an equilibrium condition is reached. A similar mechanism characterizes our system: a greater flow of drug, allowed by Equation (37), leads to a faster balance between the drug concentration in the two compartments. The equilibrium is met at shorter times, contributing to lower drug levels.

5. CONCLUSIONS AND FUTURE PERSPECTIVES

In this work, we analyze the impact of microvascular tortuosity on drug diffusion and uptake in a solid tumor. Drug dynamics are described at the tissue scale, considering both the capillary and interstitial compartments. Our modeling framework allows us to track the key drug transport properties (such as absorption and diffusion) and their dependence on the microstructure. The model derivation is based on asymptotic homogenization and exploits the sharp length separation existing between the spatial scales characterizing the tumor tissue. As a result, the geometrical information at the microscale are encoded into four tensor quantities, namely the effective hydraulic conductivities and diffusivities, which are computed via solution of three dimensional simulations defined over a single representative cell. These coefficients are then injected into the macroscale equations, which describe the evolution of drug distribution in the tumor at the tissue scale.

According to the results presented here, the model predicts impaired drug transport in the tumor for increasing geometrical complexity of the vascular network. We observe that only a small portion of the injected drug is able to reach the tumor center, due to decreased fluid convection and drug diffusion. We have investigated the effect of tortuosity on two reference molecules used by clinicians, namely Vinblastine and Doxorubicin. The results show a remarkable difference between these two drugs, due to their different interaction with the tumor interstitium. The first drug (Vinblastine) acts like a tracer molecule, with almost negligible uptake rate. In this case, the evolution of the drug is dominated by transport in the capillaries, and we observe a clear effect of tortuosity on molecule advection and diffusion. In contrast, the second molecule (Duxorubicin) is characterized by a higher uptake rate in the interstitium, and the effects of vascular network geometry on drug evolution are negligible. The observations about these molecules are confirmed by analyzing the amount of drug metabolized in the tumor, a quantity that provides a valuable index for the effectiveness of a particular therapeutic agent.

Finally, we conclude our study by introducing an additional term into the drug flux equation, accounting for convective transport of molecules through the semipermeable membrane of the capillaries. Our results show a decreased distribution of the drug within the tumor, a phenomenon similar to what is observed with fluid exchange across a malignant capillary network.

Prepared using cnmauth.cls
DOI: 10.1002/cnm

We point out that these results refer to specific anti-cancer agents and that the general problem is non-trivial due to the mutual influence of the large number of parameters involved. A sensitivity analysis leading to a more thorough understanding of model predictions would be therefore crucial to elucidate the interplay between drug transport and geometrical tortuosity for different molecules and physiological scenarios (the latter possibly involving complex, nonlinear fluid and mass exchange across the capillary walls and metabolic reactions). However, these examples clearly show that the dependence of drug transport properties on the geometrical features of the microvasculature cannot be ignored.

This work is certainly open to a number of improvements. In particular, we have assumed macroscopic uniformity to reduce computational complexity and solve the various cell problems only once for each tortuous configuration. However, in general, the tumor microvasculature is not periodic and this assumption should be relaxed to simulate a macroscopically non-periodic vascular network considering the full model [9]. In this case, one cell problem for each macroscale point should be solved, and the challenge resides in the development of efficient algorithms, which should couple macro and micro spatial variations via parallel computing together with adequate image segmentation. Alternatively, for a range of simplified microstructure, it is possible to parametrically vary the parameter(s) (such as the radius of circular objects) characterizing the microscale geometry, as done for example in [39] for advection-diffusion of solute through a macroscopically varying porous structure made of circular obstacles. Note that the solutions obtained in this work, as it usually happens for models that make use of asymptotic homogenization, are usually good over the domain interior, but may be inaccurate in regions close to the domain boundary. This could be due to a lack of y-periodicity at the border, or to other issues as reported in [40]. A possible solution for this problem can be found in [40, 41], where the authors propose a set of correctors to improve the solutions at the boundaries. The existing homogenized model should also be significantly extended to capture the nanoparticles dynamics as a drug delivery vector and their adhesion to the tortuous capillary walls. Numerical results obtained from such a model could be then compared with those presented in the context of the immersed boundary method [42] (based on the fluid transport model [43]), where a simplified, 1D representation of the vascular network is taken into account. This comparison would clarify the impact of the hydraulic properties of the microvasculature on nanomolecules adhesion.

Finally, this work represents one more significant step towards a novel framework that may improve the design and efficacy of anticancer strategies. As a next, natural step, this modeling framework and its future generalization should be applied in the context of realistic geometries obtained from medical images to enable validation of the results and provide reliable hints to the clinicians' community.

ACKNOWLEDGEMENTS

R.P. gave his major contribution to the present manuscript during his previous appointment at TU Darmstadt, where he was supported by the DFG priority program SPP 1420, project GE 1894/3 and RA 1380/7, Multiscale structure-functional modeling of musculoskeletal mineralized tissues, PIs Alf Gerisch and Kay Raum. R.P. is currently supported by the Ministry of Economy in Spain,

DOI: 10.1002/cnm

under the project reference DPI2014-58885-R, P.I. José Merodio. The authors would like to thank Toni Lassila for the kind invitation to the mini-symposium on "Multiscale Modelling of Transport Phenomena in Biological Tissue", held in Cachan, in the context of the CMBE2015 workshop, and the CMBE2015 organizing co-chairs and committees for the inviting us to submit the present special issue. The authors are indebted to Davide Ambrosi and Rebecca J. Shipley for useful discussions concerning the content of this work.

REFERENCES

1. Carmeliet P, Jain RK. Angiogenesis in cancer and other diseases. *Nature* 2000; **407**(6801):249–257.
2. Stylianopoulos T, Martin JD, Snuderl M, Mpekris F, Jain SR, Jain RK. Coevolution of solid stress and interstitial fluid pressure in tumors during progression: implications for vascular collapse. *Cancer research* jul 2013; **73**(13):3833–41.
3. Jain RK. Determinants of tumor blood flow: a review. *Cancer research* may 1988; **48**(10):2641–58.
4. Minchinton AI, Tannock IF. Drug penetration in solid tumours. *Nature reviews. Cancer* aug 2006; **6**(8):583–92.
5. Jain RK, Stylianopoulos T. Delivering nanomedicine to solid tumors. *Nature reviews. Clinical oncology* nov 2010; **7**(11):653–64.
6. Jain RK. Physiological barriers to delivery of monoclonal antibodies and other macromolecules in tumors. *Cancer research* feb 1990; **50**(3 Suppl):814s–819s.
7. Chaplain MAJ, McDougall SR, Anderson ARA. Mathematical modeling of tumor-induced angiogenesis. *Annual review of biomedical engineering* jan 2006; **8**:233–57.
8. Kim M, Gillies RJ, Rejniak Ka. Current Advances in Mathematical Modeling of Anti-Cancer Drug Penetration into Tumor Tissues. *Frontiers in oncology* jan 2013; **3**(November):278.
9. Penta R, Ambrosi D, Quarteroni A. Multiscale homogenization for fluid and drug transport in vascularized malignant tissues. *Mathematical Models and Methods in Applied Sciences* 2015; **25**(01):79–108.
10. Mei CC, Vernescu B. *Homogenization Methods for Multiscale Mechanics*. World Scientific, 2010.
11. Kedem O, Katchalsky A. Thermodynamic analysis of the permeability of biological membranes to non-electrolytes. *Biochimica et biophysica Acta* 1958; **27**:229–246.
12. Kedem O, Katchalsky A. Thermodynamic analysis of the permeability of biological membranes to non-electrolytes. 1958. *Biochimica et biophysica acta* 1989; **1000**:413–30.
13. Penta R, Ambrosi D. The role of the microvascular tortuosity in tumor transport phenomena. *Journal of Theoretical Biology* 2015; **364**:80–97.
14. Shipley RJ, Chapman SJ. Multiscale modelling of fluid and drug transport in vascular tumours. *Bulletin of Mathematical Biology* 2010; **72**(6):1464–1491.
15. Penta R, Mascheroni P. The role of the angiogenic network structure on diffusion and consumption of anti-cancer drugs. *4th International Conference on Computational and Mathematical Biomedical Engineering - CMBE2015*, 2015; 186–189.
16. Sanchez-Palencia E. *Homogenization method for the study of composite media*, *Lecture Notes in Mathematics*, vol. 985. Springer Berlin Heidelberg, 1983.
17. Holmes MH. *Introduction to Perturbation Methods*, *Texts in Applied Mathematics*, vol. 20. Springer Berlin Heidelberg, 1995.
18. Waniewski J. Mathematical modeling of fluid and solute transport in hemodialysis and peritoneal dialysis. *Journal of Membrane Science* 2006; **274**(1-2):24–37.
19. Penta R, Ambrosi D, Shipley RJ. Effective governing equations for poroelastic growing media. *The Quarterly Journal of Mechanics and Applied Mathematics* 2014; **67**(1):69–91.
20. Jain RK, Tong RT, Munn LL. Effect of Vascular Normalization by Antiangiogenic Therapy on Interstitial Hypertension, Peritumor Edema, and Lymphatic Metastasis: Insights from a Mathematical Model. *Cancer Research* 2007; **67**(6):2729–2735.
21. Boucher Y, Brekken C, Netti Pa, Baxter LT, Jain RK. Intratumoral infusion of fluid: estimation of hydraulic conductivity and implications for the delivery of therapeutic agents. *British journal of cancer* 1998; **78**(11):1442–8.
22. Rand PW, Lacombe E, Hunt HE, Austin WH. Viscosity of normal human blood under normothermic and hypothermic conditions. *Journal of Applied Physiology* 1964; **19**(1):117–122.

Prepared using cnmauth.cls
DOI: 10.1002/cnm

23. Less JR, Posner MC, Skalak TC, Wolmark N, Jain RK. Geometric resistance and microvascular network architecture of human colorectal carcinoma. *Microcirculation* 1997; **4**(1):25–33.
24. Hahnfeldt P, Panigrahy D, Folkman J, Hlatky L. Tumor Development under Angiogenic Signaling : A Dynamical Theory of Tumor Growth , Treatment Response , and Postvascular Dormancy Advances in Brief Tumor Development under Angiogenic Signaling : A Dynamical Theory of Tumor. *Cancer Res* 1999; **59**:4770–4775.
25. Modok S, Hyde P, Mellor HR, Roose T, Callaghan R. Diffusivity and distribution of vinblastine in three-dimensional tumour tissue: Experimental and mathematical modelling. *European Journal of Cancer* 2006; **42**(14):2404–2413.
26. Modok S, Scott R, Alderden Ra, Hall MD, Mellor HR, Bohic S, Roose T, Hambley TW, Callaghan R. Transport kinetics of four- and six-coordinate platinum compounds in the multicell layer tumour model. *British journal of cancer* 2007; **97**(2):194–200.
27. Jain RK, Baxter LT. Mechanisms of heterogeneous distribution of monoclonal antibodies and other macromolecules in tumors: Significance of elevated interstitial pressure. *Cancer Research* 1988; **48**(24 I):7022–7032.
28. Nelson R, Dyke R, Root M. Comparative pharmacokinetics of vindesine, vincristine and vinblastine in patients with cancer. *Cancer Treatment Reviews* sep 1980; **7**:17–24, doi:10.1016/S0305-7372(80)80003-X.
29. Karatasos K. Self-Association and Complexation of the Anti-Cancer Drug Doxorubicin with PEGylated Hyperbranched Polyesters in an Aqueous Environment. *The Journal of Physical Chemistry B* feb 2013; **117**(8):2564–2575.
30. Weinberg BD, Patel RB, Exner Aa, Saidel GM, Gao J. Modeling doxorubicin transport to improve intratumoral drug delivery to RF ablated tumors. *Journal of Controlled Release* dec 2007; **124**(1-2):11–19.
31. Eikenberry S. A tumor cord model for Doxorubicin delivery and dose optimization in solid tumors. *Theoretical Biology and Medical Modelling* 2009; **6**(1):16.
32. Rahman A, Ganjei A, Neefe J. Comparative immunotoxicity of free doxorubicin and doxorubicin encapsulated in cardiolipin liposomes. *Cancer Chemotherapy and Pharmacology* jan 1986; **16**(1):28–34.
33. Dawidczyk CM, Kim C, Park JH, Russell LM, Lee KH, Pomper MG, Searson PC. State-of-the-art in design rules for drug delivery platforms: lessons learned from FDA-approved nanomedicines. *Journal of controlled release : official journal of the Controlled Release Society* aug 2014; **187**:133–44.
34. Perktold K, Prosi M, Zunino P. Mathematical models of mass transfer in the vascular walls. *Cardiovascular Mathematics*, *MS&A*, vol. 1, Formaggia L, Quarteroni A, Veneziani A (eds.). Springer Milan, 2009; 243–278.
35. Rahman A, Treat J, Roh J, Potkul L, Alvord W, Forst D, Woolley P. A phase I clinical trial and pharmacokinetic evaluation of liposome-encapsulated doxorubicin. *Journal of clinical oncology : official journal of the American Society of Clinical Oncology* 1990; **8**(6):10931100.
36. Neville AJ, Rand CA, Barr RD. Vinblastine-induced erythrocytotoxicity. *Scandinavian Journal of Haematology* 1982; **28**(1):32–38.
37. Zhou XJ, Rahmani R. Preclinical and Clinical Pharmacology of Vinca Alkaloids. *Drugs* 1992; **44**(Supplement 4):1–16.
38. Tacar O, Sriamornsak P, Dass CR. Doxorubicin: an update on anticancer molecular action, toxicity and novel drug delivery systems. *Journal of Pharmacy and Pharmacology* 2013; **65**(2):157–170.
39. Dalwadi MP, Griffiths IM, Bruna M. Understanding how porosity gradients can make a better filter using homogenization theory. *Proc. R. Soc. A*, vol. 471, The Royal Society, 2015; 20150 464.
40. Lefik M, Schrefler BA. Fe modelling of a boundary layer corrector for composites using the homogenization theory. *Engineering Computations* 1996; **13**(6):31–42.
41. Lefik M, Schrefler BA. Modelling of nonstationary heat conduction problems in micro-periodic composites using homogenisation theory with corrective terms. *Archives of Mechanics* 2000; **52**(2):203–223.
42. Cattaneo L, Zunino P. A computational model of drug delivery through microcirculation to compare different tumor treatments. *International journal for numerical methods in biomedical engineering* 2014; **30**(11):1347–1371.
43. Cattaneo L, Zunino P. Computational models for fluid exchange between microcirculation and tissue interstitium. *Networks & Heterogeneous Media* 2014; **9**(1).

DOI: 10.1002/cnm